



## ORIGINAL PAPER

## ANALYSIS OF CYLINDRICAL TUNNELS UNDER COMBINED PRIMARY NEAR FAULT SEISMIC EXCITATIONS AND SUBSEQUENT REVERSE FAULT RUPTURE

Mahsa GHARIZADE VARNUSFADERANI<sup>1)</sup>, Aliakbar GOLSHANI<sup>2)</sup> \*and Sina MAJIDIAN<sup>1)</sup><sup>1)</sup> Geotechnical Engineering, Faculty of Civil and Environmental Engineering, Tarbiat Modares University, Tehran, Iran<sup>2)</sup> Faculty of Civil and Environmental Engineering, Tarbiat Modares University, Tehran, Iran\*Corresponding author 's e-mail: [golshani@modares.ac.ir](mailto:golshani@modares.ac.ir)

## ARTICLE INFO

## Article history:

Received 5 January 2016

Accepted 30 June 2016

Available online 22 August 2016

## Keywords:

Finite element method

Near-field ground motions

Fault slip

Tunnel lining deformation

Sectional forces in tunnel lining

## ABSTRACT

An earthquake fault rupture generates two types of ground motion: permanent quasi-static dislocations and dynamic oscillations, characterized by strong pulses. This study investigates tunnel's response to two different conditions using a 2D finite element program; the first one has a static dislocation corresponding to different earthquake magnitudes, while the second combines near-field seismic motions with three specific peak ground accelerations along with permanent dislocations.

The impulsive ground motions affect the lining response further to other influential factors such as fault type and dip angle, making changes in sectional forces, displacement, and shear distortion of the lining. Moreover, pulse intensity, period, and frequency content are effective characteristics of impulsive motions that change in final response of the lining, subjected to subsequent static dislocations. Based on the second condition, at low PGAs, the pulse type is more effective to final response of the lining, due to forward and backward momentum specifications in impulsive motions. For earthquakes with high PGA and larger values in near-field parameters, both the pulse type and period are effective. The tunnel displacement increases at PGAs as large as 0.7 and 1g, unlike the low PGA as large as 0.35g, because of increasing soil stress and plastic strain, respectively.

## 1. INTRODUCTION

Recent earthquakes such as the one in Kobe 1995 (Japan), Chi-Chi 1999 (Taiwan), and Niigata 2004 (Japan) demonstrated that underground structures are vulnerable to earthquakes and the associated risk may be high, since even a low level of damage may affect their serviceability. These damages are categorized by Dowding and Rozen (1978) into three main categories, with regards to the earthquake, itself:

Damage from ground shaking

Damage from fault dislocation

Damage by earthquake-induced ground failures (e.g., liquefaction and landslides).

The seismic damages suffered by underground structures show that most tunnels were located in the vicinity of causative faults (Corigliano, 2007). The specifications of near field ground motion are significantly different from that of the far-field. The ground motion close to an active fault may be characterized by strong pulses and is severely influenced by the rupture mechanism, the direction of rupture propagation relative to the site as well as to possible permanent ground displacement resulting from a fault slip. These latter two phenomena are usually referred to as “rupture-directivity” and “fling

step” effects, respectively. For a dip-slip earthquake (i.e., reverse or normal earthquake), both of the dynamic and static dislocation occur on the strike-normal component with a little motion on the strike-parallel component. If the static ground displacement is removed from the strike-normal component, there remains a large directivity pulse. On the contrary, for a strike-slip earthquake, the rupture directivity pulse and the static ground displacement are partitioned on the strike-normal and strike-parallel components, respectively. If the static ground displacement is removed from the strike-parallel component, a very small dynamic motion remains. (Somerville, 2002). For a strike-slip faulting, the impact of directivity on amplitudes is weak in the epicenter's vicinity. In contrast, for dip-slip faults, the same effect is large in the region located around the epicenter (Somerville et al., 1997). The dip-slip mechanisms and the orientation of rupture directivity pulse and fault displacement are shown in Figure 1 and Figure 2, respectively.

Lack of recommendations for an underground structure designing, influenced by fault movement, have forced the researchers to study their behavior using numerical analysis and experimental methods. Some researchers studied the impact of fault rupture on tunnels. Lin et al. (2007) established a full-scale

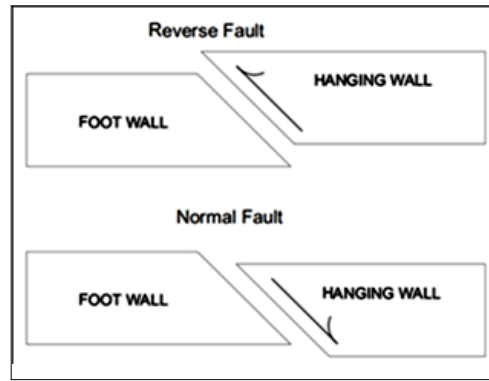


Fig. 1 Schematic mechanisms of dip-slip fault types.

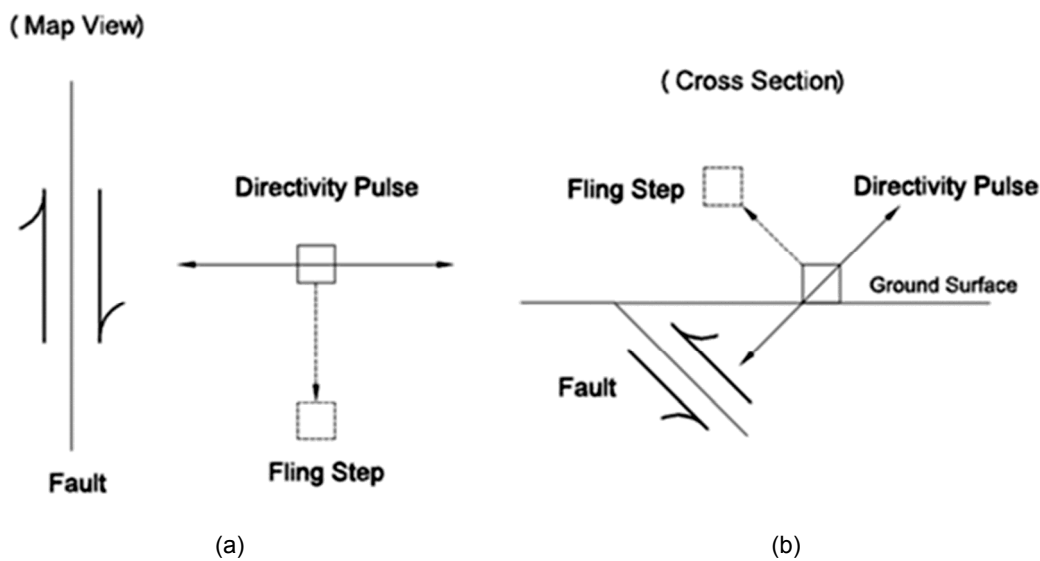


Fig. 2 Schematic orientation of rupture directivity pulse and fault displacement (fling step) for (a) strike slip and (b) dip slip faulting (Somerville, 2002).

numerical model for tunnels, based on a calibrated small-scale model, in a line with the model experiments. They studied the effects of thrust faulting at an angle of  $60^\circ$  on a cylindrical tunnel section under different soil parameters and tunnel positions toward fault rupture (Lin et al., 2007). They found that the existence of the tunnel and its location influence the development of a shear zone in the soil. A fault zone developed by thrust fault will induce the failure of the lining, especially for tunnels located inside the shear zone. Furthermore, the soil stress and load in the lining will also be significantly affected by the potential occurrence of a back-thrust shear zone. Based on their study, the soil properties, especially the stiffness, affect the development of shear zones, back-thrust, and the safety of the lining as well. Also, Anastasopoulos and Gazetas (2010) studied the effects of normal faults rupture on cut-and-cover tunnels. They found that, in all cases investigated, the rupture path is severely affected by existence of the tunnel. Due to the developing interaction between the tunnel and the rupture, the imposed deformation of faulting

is converted to a diffuse differential displacement acting at the base of the tunnel. Depending on the position of the tunnel with respect to the emerging fault rupture, the structure may be subjected either to hogging deformation or to sagging deformation. Also, they found that the overburden soil has a dual role such that it pushes the tunnel to compress the soil underneath; and also, it increases the confining stresses underneath the tunnel, thus it facilitates the bifurcation of the fault zone. Generally, soil compliance is beneficial for the distress of the tunnel during the fault rupture, but not necessarily for its rotation. Also, Gharizade Varnusfaderani et al. (2015) studied the behavior of circular tunnels crossing active normal and reverse fault rupture with different earthquake magnitudes and fault dip angles. In their research, the lining location varied relative to the fault tip line and it is structurally discussed. They found that the magnitude of the bending moment induced in lining section, corresponding to the tunnels located in footwall, for all reverse fault dip angles, is greater than the one in the normal faults. The magnitude of

the axial load corresponding to the tunnels located near the fault in footwall, under reverse fault dip angles lower than  $60^\circ$ , is greater than the one in normal fault and it is the opposite for angles larger than  $60^\circ$ . The horizontal and vertical displacements occurred for the tunnel located in footwall, in each reverse fault dip angle is greater than the one in normal fault.

Beside these studies, there are some studies on impact of both permanent fault displacement and strong ground motions or each one individually. To mention a couple, Anastasopoulos et al. (2008a) and Corigliano et al. (2011) studied the behavior of tunnel in near field conditions. In the first research paper, the authors parametrically explored three possible segment lengths with two types of joint for a 70 m deep immersed tunnel. They concluded that in all analyzed cases for the joints between segments that were differentially deformed after the quasi-static fault rupture, upon subsequent very strong seismic shaking, overstressed joints de-compress and understressed joints re-compress. This process leads to a more uniform deformation profile along the tunnel. This is particularly beneficial for the precariously de-compressed joint gaskets. Hence, the safety of the immersed tunnel improves with "subsequent" strong seismic shaking.

In the second research, the authors studied the seismic analysis of deep tunnels in near fault conditions, based on a case study in Southern Italy. This study focused on improving the method currently used for a seismic analysis of underground structures in near field condition. The seismic response in the transversal direction had been analyzed by using the pseudo-static approach as well as advanced numerical modeling. From the analyses, it turned out that the estimation of the dynamic increment of the internal forces in the lining can be obtained in a simplified way by estimating the earthquake-induced ground strain assuming free-field conditions and the obtained results are reasonable from an engineering point of view.

The current paper aims at studying the deformation and sectional forces in a specific tunnel lining under the influence of near field earthquakes including permanent displacement induced by the reverse fault slip and subsequent dynamic strong ground motions. It is assumed that the tunnel near a major active fault, is first influenced by strong ground motions originating at a different major fault located in the vicinity of the site (i.e., less than 10 km) and then the tunnel was influenced by a fault dislocation. In more details, the subsequent fault rupture was motivated by the near field seismic excitation. Accordingly, a nonlinear finite-element methodology (FEM) was first developed to study the tunnel behavior under the first mentioned effect of faulting (fault slip) and then to study under the combination of both effects (i.e., fault dislocation and dynamic ground movement due to rupture directivity). Hence

the tunnel model motivated by primary strong motions is then subjected to static reverse fault slip. In this study, a tunnel with specific lining section was evaluated under both the quasi-static fault dislocation and seismic near fault excitations. Also, concerning the seismic investigations, just three specific PGAs as high as 0.35, 0.7, and 1g were considered. Since being close to the presented study the investigation carried out by Lin et al. (2007) is selected here as the reference one. Accordingly, the model configuration and the material properties are adopted from their study.

## 2. METHODOLOGY

### 2.1. STEPS OF ANALYSIS

In this research, the FEM based commercial code ABAQUS 6-10.1 (2010) was adopted for the numerical analysis carried out in four steps:

- In "step 1" the in-situ geostatic stresses were modeled, with the coefficient for lateral soil pressure assumed to be  $K_0 = 1 - \sin \varphi$  (Jacky, 1944).
- In "step 2" the tunnel excavation was modeled. The tunneling is a TBM based excavation. The numerical model is based on stress release ratio method. In this way, when the equilibrium of in-situ stresses was reached, the soil in the tunnel section was removed with a relaxation factor of 40 percent, followed by the installation of segmental tunnel lining. Removing the tunnel section and installing simultaneously the tunnel lining, leads to support forces that are 50 % to 100 % overestimated (Einstein and Schwartz, 1979). The possibility of occurrence of deformations around the tunnel leads to the reduction of supporting forces. Therefore, in this study, considering real excavation and three dimensional modeling effects, the results of two and three dimensional tunnel excavation models such as tunnel vault and invert displacement (i.e., the measure of convergence at the tunnel section) and stress state around the tunnel opening were compared by means of a finite-element method based on 2D and 3D tunnel models. In fact, the measured displacements in 3D tunnel model were then created in 2D tunnel model by considering a relaxation factor applied to the soil around the tunnel opening. Accordingly, comparing these two models, the 40 % as relaxation factor was adopted for 2D tunnel model (see the Appendix A).
- In "step 3" the displacement time histories based on three selected near field records were applied to the bedrock. Actually, the boundary condition varied with time, based on the displacement time history. As mentioned previously, the seismic excitations originated at different active faults located in the vicinity of the site (i.e. at distance less than 10 km). The selected time histories

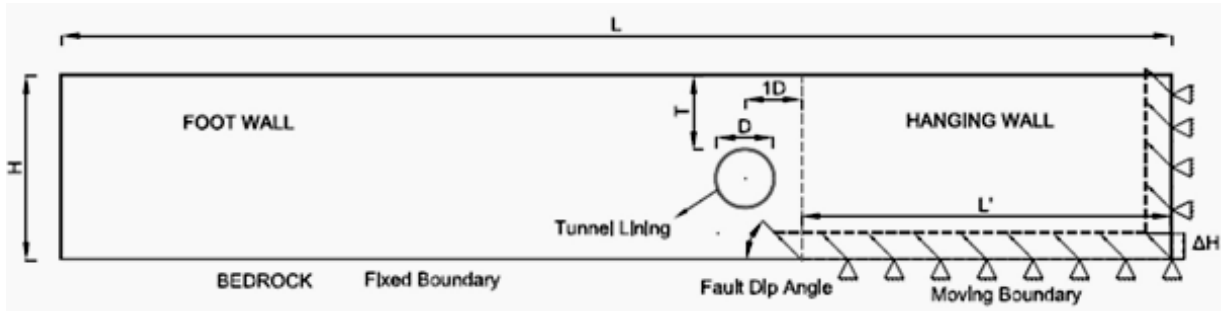


**Fig. 3** Illustration of the tunnel configuration, fault rupture, boundary conditions, and fault dip angle adopted for numerical study of quasi -static fault rupture (Lin et al., 2007). The tunnel is located at footwall side and the center of circular tunnel lining is at a distance  $1D$  from the fault tip line, which is shown as dotted.

should have some specific conditions. More details are given in Section 2-3. It should be noted that a rigid area similar to rock materials developed at the bottom of the model. This prevents from occurrence of excessive distortion in numerical analysis, during the seismic excitation and fault dislocation in step 4. Also, this area is sufficiently rigid not to change the input seismic and static excitations.

- Finally, in “step 4” the fault slip was applied by changing boundary conditions and making upward displacement in hanging wall side to simulate reverse fault rupture. This step was considered to simulate fault dislocations following the near fault earthquakes. More details are given in Section 2-4. In fact, both the fixed boundary conditions at the bottom and rolling conditions at the side of the hanging wall were changed to moving boundary conditions composed of horizontal and vertical displacement with the assumed fault dip angle, see Figure 1. By the reverse fault slip, the hanging wall moves left and upward.

## 2.2. MODEL PROPERTIES

The tunnel’s full-scale model corresponds to an actual shield tunnel in the Taipei metro system, running close to the Taipei fault with a varied distance (Lin et al., 2007 and Chung et al., 2005). Figure 3 provides the configuration of this tunnel, fault rupture, boundary conditions, and fault dip angle adopted for the numerical study. Simulating the reverse fault movement, the fixed boundary conditions at the right side of the model (hanging wall side) were changed to the moving upward conditions. Not having complete information about an accurate distance of a fault line to the tunnel axis, it is reasonable to study this structure at different locations relative to the assumed fault tip line. Table 1 presents a summary of the soil and lining parameters. An elastic perfectly plastic constitutive model, with the Mohr - Coulomb failure criterion for the soil material and a linear elastic behavior were adopted for the tunnel lining. The model dimensions are shown in Table 2. Based on

**Table 1** Summary of the material properties considered in this study (Lin et al., 2007).

Parameters		Unit
Lining model	$E_s$	31800 <i>MPa</i>
	$\nu_s$	0.2 -
Soil model	$\gamma$	20 <i>N/m<sup>2</sup></i>
	$E$	19 <i>MPa</i>
	$\nu$	0.3 -
	$c$	5 <i>kPa</i>
	$\phi$	30 -
	$\psi$	6.30 -

*Remark:*

$E$ : Elasticity modulus,  $\nu_s$ : Poisson ratio,  $\gamma$ : Specific density,  $c$ : Cohesion,  $\phi$ : Friction angle,  $\psi$ : Dilation angle.

**Table 2** Summary of the model dimensions (Lin et al., 2007).

Parameters	dimensions	Unit
$L$	1000	<i>m</i>
$H$	20	<i>m</i>
$T$	11	<i>m</i>
$D$	6.1	<i>m</i>
$L'$	400	<i>m</i>

*Remark:*

$L$ : length of numerical model,  $H$ : depth of soil,  $T$ : tunnel depth,  $D$ : Tunnel diameter,  $L'$ : length of hanging wall.

given information in Table 2, the model’s length was enlarged to reduce seismic reflected waves. Accordingly, the accuracy of its dimensions was checked by a sensitivity analysis, based on achieving uniform variations in displacement contours in the model. Figure 4 shows the configuration of tunnel lining. Basically, in engineering practice a complete concrete lining is composed of segments and joints. In order to account for joint existence, the tunnel lining was considered as a continuous ring with a discounted rigidity of lining at a joint position (Muir Wood, 1975;

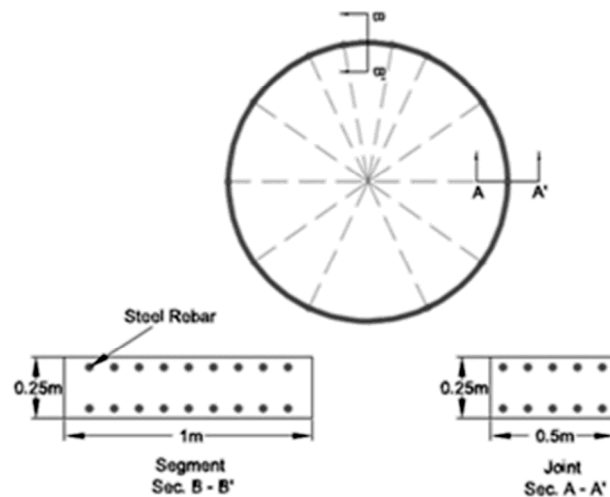


**Fig. 4** Typical setup of the segmental lining. A complete circular ring is formed by 12 segments and joints. (a) cross-section B-B' at segment. (b) equivalent cross section at joint A-A' (Lin et al., 2007).

Lee et al., 2001b; ITA, 2000). The hypothetical shield tunnel consists of twelve segments and joints with the discounted rigidity of the tunnel lining at the joints modeled by reducing half of the beam cross section (Lin et al., 2007). The segments and joint sections were 1.0 and 0.5 m long, respectively and 0.25 m wide (see Fig. 4). The joints were considered to have a small length in complete ring, as high as 5 cm, and they were tied to the segments.

The ground mass was modeled using the two-dimensional plane strain using quadrilateral elements with the capability of updating mesh. This capability helps not to have excessive distortion in elements during large deformation. The tunnel lining was represented by linear elastic beam elements. Concerning the soil-tunnel lining interaction, interface elements were employed. To that end, a tangential behavior with friction coefficient of 0.36 ( $\mu = \tan(2\phi/3)$ ) and a normal behavior with an allowable nodal separation was adopted (Lin et al., 2007).

### 2.3. SELECTION OF SEISMIC RECORDS FOR TIME HISTORY ANALYSIS

Near fault earthquake records have some special characteristics that differ from far field conditions. There is some definition for these records. For example, Martinez-Pereira and Bommer (1998) inspected various definitions of near fault zone. Based on their study, all these definitions should satisfy several criteria at specific lower limit values (ibid). Maniatakis et al. (2008) identified the near fault earthquake record characteristics using a procedure. In this procedure, some parameters for identification of near fault records are derived or calculated corresponding to the record specifications. The

mentioned parameters are including peak horizontal ground velocity ( $PGV$ ), cumulative absolute velocity ( $CAV$ ), arias intensity ( $I_A$ ), and the root mean square acceleration ( $a_{rms}$ ), all of which have to satisfy a lower bound values shown in Table 4. These parameters indicate the complexity of strong ground motion, such as frequency content, amplitude, and duration of motion. This suggests that no single parameter can describe strong ground motion accurately (Jennings, 1985). Usually, the near fault zone is considered to be within an epicentral distance of about 20-60 km from the fault rupture (Stewart et al., 2001). However, at distances lower than 15-25 km, underground structures are vulnerable to these seismic excitations. Therefore, in this paper the selected seismic records were within a distance lower than 10 km and with reverse fault mechanism. Based on this identification procedure, six near-fault earthquake time histories were compiled and then distinguished based on the pulse type. Finally, from all time histories, three ones representing a specific pulse characteristic were selected to be applied directly to the model. In the following, it is explained in details that how and why these pulse types are selected.

The characteristics of the impulsive nature of near fault ground motions affect seismic design (Mavroeidis and Papageorgiou, 2003). The directivity-pulses are dynamic effects of near-fault excitations. The term "directivity pulse" usually refers to "forward directivity pulses", which are more critical to engineered structures (Cox and Ashford, 2002). The impulsive characteristic of near-fault records is not always apparent in the acceleration time history, while an accurate examination of the velocity and displacement time histories of these records

**Table 3** Average permanent displacement (Wells and Coppersmith, 1994).

Fault type	Dip angle	component	Average displacement (m)		
			Mw(6)	Mw(6.5)	Mw(7)
R	Total slip		0.550	0.603	0.661
	45	H	0.389	0.426	0.476
		V	0.389	0.426	0.476
	60	H	0.275	0.302	0.331
		V	0.476	0.522	0.572
	75	H	0.142	0.156	0.171
V		0.531	0.582	0.638	

Remark:

R: Reverse fault type,  $M_w$ : Earthquake magnitude,

H: Horizontal component of fault dislocation,

V: Vertical component of fault dislocation,

Dip angle is in degree and relative to the horizontal direction.

**Table 4** Near fault ground motion parameters and the lower-bound values (Martinez-Pereira and Bommer, 1998)

Ground motion parameters	Lower- bound
PGA	0.2 g (m/s <sup>2</sup> )
CAV	0.3 g. sec (m/s)
PGV	20 (cm/sec)
$I_A$	0.4 (m/s)
$a_{rms}$	0.5 (m/sec <sup>2</sup> )

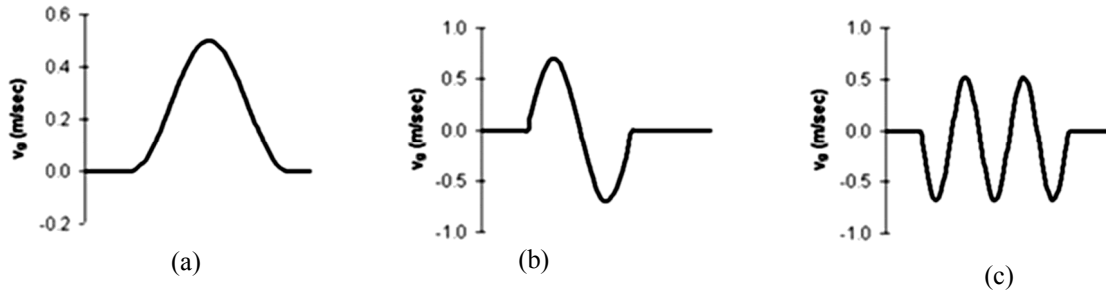
Remarks:

PGA: Peak Ground Acceleration, CAV:

Cumulative Absolute Velocity, PGV: Peak

Ground Velocity,  $I_A$ : Arias Intensity,  $a_{rms}$ :

Root Mean Square Acceleration.

**Fig. 5** Schematic representation of velocity time history for: (a) Pulse type-A, (b) Pulse type-B, and (c) Pulse type-C2; in diagram,  $V_g$  in vertical axis refers to an alternative of ground velocity and the horizontal axis is the time.

reveals the special nature of the pulse-like motion due to forward directivity (Bray and Rodriguez-Marek, 2004). It has been proved that the equivalent pulses are capable of representing near-fault ground motion while the accuracy of such representation is not equally good in all cases (Alavi and Krawinkler, 2000). Following the mentioned procedure, the velocity pulses were categorized to three types as Type-A, Type-B, and Type-C<sub>n</sub> (Makris, 1997), as shown in Figure 5. Evaluating and categorizing the equivalent pulse types needs to calculate the following parameters:

- The maximum ratio of spectral velocity to peak ground velocity ( $SV_{max}/PGV$ ) for 5 % damping ( $\xi=0.05$ ), as used by Maniatakis et al. (2008). In other words, this normalized index facilitates the correlation between the recorded strong motion and the pulse type (i.e., the mentioned A, B, and C<sub>n</sub> pulses) (Maniatakis et al., 2008). Also, the fault characteristics and the fault slip distribution are attributed to the number of half-sine waves in the velocity time history (Somerville et al., 1997; Bray and Rodriguez-Marek, 2004). Based on the previous studies, the equivalent pulse velocity lies within 20% of the peak ground velocity of the

record. Thus, the peak ground velocity appears to be a simple and stable measure of the pulse severity (Alavi and Krawinkler, 2000).

- The predominant period  $T_p$ , corresponds to the maximum spectral velocity (SV) for  $\xi=0.05$ , as defined by Krawinkler and Alavi (1998) and used by Maniatakis et al. (2008). This parameter is defined as the duration of a complete velocity cycle. According to Bray and Rodriguez-Marek (2004), the period of the velocity pulse  $T_p$  is a function of the moment magnitude related with the duration of the velocity pulse with the largest amplitude.

Findings show that the pulse-like motions due to forward rupture directivity amplify the spectral scaling factors of the displacement (Bommer and Mendis, 2005). Based on a study of the effects from rupture directivity on ground motion attenuation relationships, the pulse period increases with earthquake magnitude, a parameter related to fault dimensions and source parameters (Somerville, 2003). Thus, the amplification effect of impulsive motion is limited to a narrow region near the prominent period of the pulse. Figures 5 and 6 present the velocity time history and the limits of  $SV_{max}/PGV$  versus

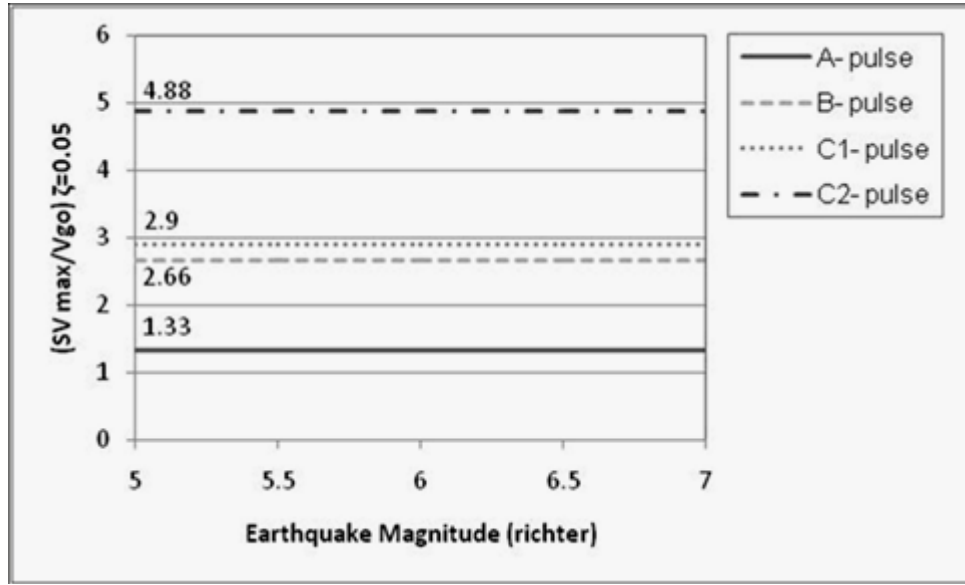


**Fig. 6** The maximum ratio of spectral velocity to peak ground velocity for  $\xi=0.05$ ;  $V_{go}$  refers to an alternative of PGV (Maniatakis et al., 2008).

**Table 5** The selected time histories of near fault earthquake records.

Earthquake	Fault type	$M_w$	Distance (km)	PGA (m/s <sup>2</sup> )	PGV (cm/s)	CAV (m/s)	$I_A$ (m/s)	$a_{rms}$ (m/s <sup>2</sup> )	$T_p$	$SV_{max}$ (cm/s)	$SV_{max}/PGV$
Cape-Mendocino W	R	7.1	9	1.04 g	41.28	10.15	2.388	0.072 g	2.34	99.75	2.42
Loma-Prieta-gilroy arraye-W	R	6.9	10.5	0.473 g	33.87	7.31	1.679	0.052 g	0.41	126.82	3.74
Northridge-Pacoima dam-W	R	6.7	8	1.285 g	103.53	18.45	8.597	0.118 g	0.92	231.21	2.23

Remarks:

R: Reverse Fault,  $M_w$ : Earthquake Magnitude (Richter), PGV: Peak Ground Velocity, CAV: Cumulative Absolute Velocity,  $I_A$ : Arias Intensity,  $a_{rms}$ : root mean square acceleration,  $T_p$ : Pulse period,  $SV_{max}$ : maximum spectral velocity

earthquake magnitudes, according to the different pulse types, respectively. As shown in Figures 6, the type-A pulses have the lowest values of the  $SV_{max}/PGV$  ratio (Maniatakis et al., 2008). The permanent displacement of faulting (fling-step) is related to type-A velocity pulses. In fact, by dip-slip faulting, a combination of directivity-pulse and fling-step occurs in a horizontal direction (Stewart et al., 2001). As mentioned previously, the two effects of near-fault earthquakes are applied in two separate steps to study both effects. Since this section focused on dynamic effects of near fault earthquakes, there is no effect of permanent fault displacement on the selected records due to the fault slip. Based on the previously specified lower limit values (Table 4), and the obtained parameters including, the maximum ratio of spectral velocity of the records for 5 % damping ( $\xi=0.05$ ) and the predominant period, three seismic records were selected with pulse types B and C (in fact, with forward rupture directivity effect) for the time history analysis (Table 5). These records have been downloaded from PEER Strong Motion Database. Here, the seismic analysis is based on

displacement time history, corresponding to the recorded acceleration time history. It should be noted that the acceleration time histories are first proportionate to PGAs 0.35g, 0.7g and 1g and then the displacement time histories are derived from (see Appendix B). The seismic excitation lasted for 17 seconds and applied to the bedrock (Fig. 7).

#### 2.4. PERMANENT FAULT DISPLACEMENT

The relationships between the dynamic and permanent components of near-fault ground displacements are quite complex. As mentioned previously in Section 1, for a dip-slip earthquake (i.e., reverse or normal earthquake), both of the dynamic and static dislocation occur on the strike-normal component with a little motion on the strike-parallel component. If the static ground displacement is removed from the strike-normal component, there remains a large directivity pulse. On the contrary, for a strike-slip earthquake, the rupture directivity pulse and the static ground displacement are partitioned on the strike-normal and strike-parallel components, respectively. If the static ground displacement is

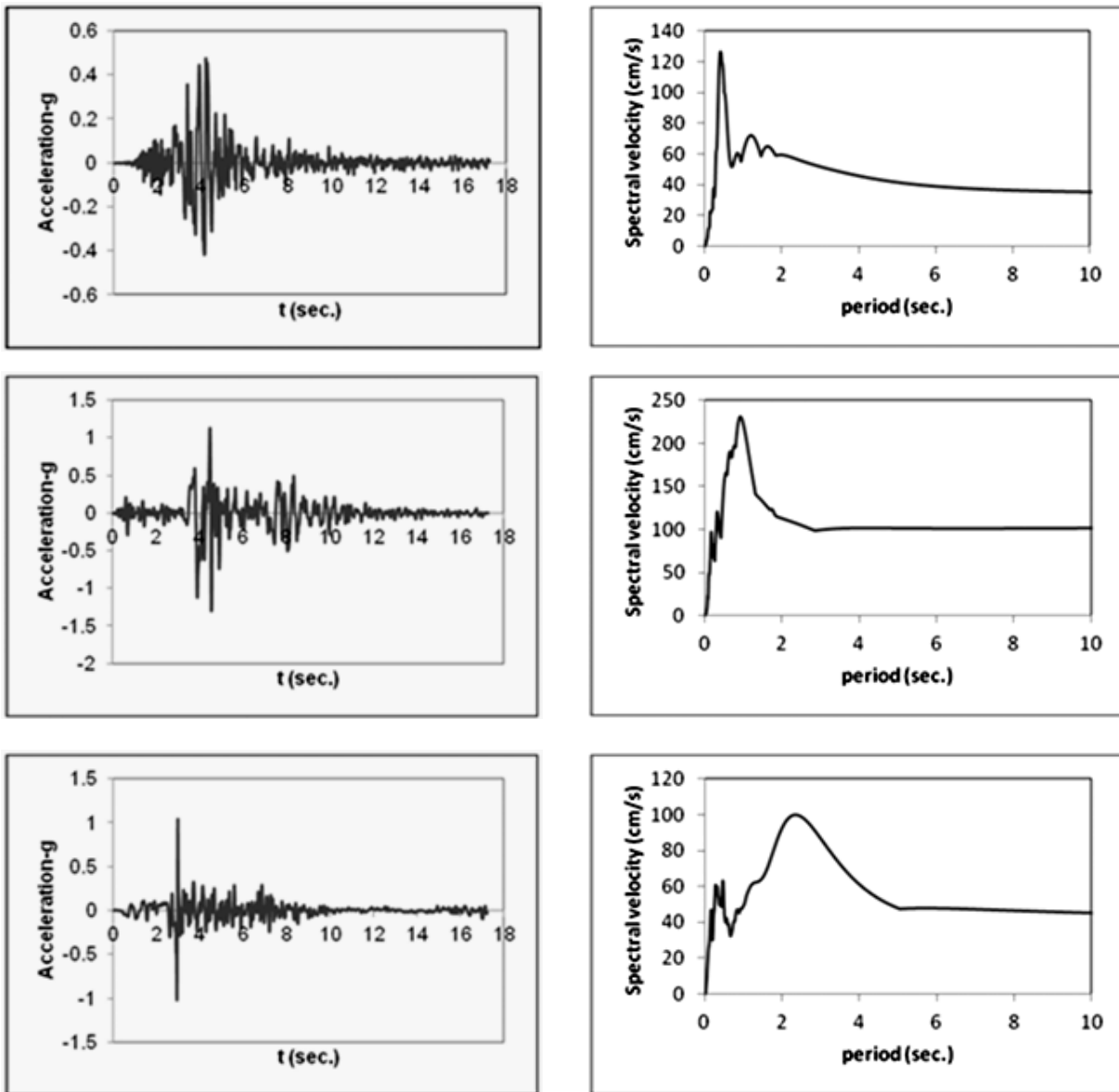


Fig. 7 The time history of accelerations and spectral velocity for the selected earthquakes (a) Loma-Prieta (b) Northridge (c) Cape-Mendocino.

removed from the strike-parallel component, a very small dynamic motion remains. This indicates that separate models are needed for predicting the dynamic and permanent components of near-fault ground displacements at a site. The separately estimated dynamic and permanent components of the ground motion can be combined to produce ground motion time histories representing both effects (Somerville, 2002). The permanent fault displacement can be estimated by empirical models (e.g., Wells and Coppersmith, 1994).

Wells and Coppersmith (1994) have collected a data base of source parameters for 421 historical earthquakes, publishing new empirical relationships in relation to earthquake magnitudes to surface rupture length, subsurface rupture length, maximum rupture area, and average fault displacement. Using these

relationships, the average reverse fault displacements for earthquakes with magnitudes of 6.0, 6.5, and 7.0 Richter, were obtained (Table 3).

## 2.5. VERIFICATION OF THE FULL-SCALE NUMERICAL MODEL

A full-scale numerical model was established based on Lin et al. (2007) and the modeling method validated through qualitative (zone of plastic shear strain) and quantitative ( $P$ - $M$  curve for tunnel lining) comparisons. The primary modeling procedure corresponds to the first and second steps (mentioned in Section 2-1) to create initial condition, and then, fault dislocation applied to the model according to the forth step with Lin et al.'s assumptions. Lin et al.'s study was based on a case study on the response of shield tunnel near a thrust fault offset by Chung et al.

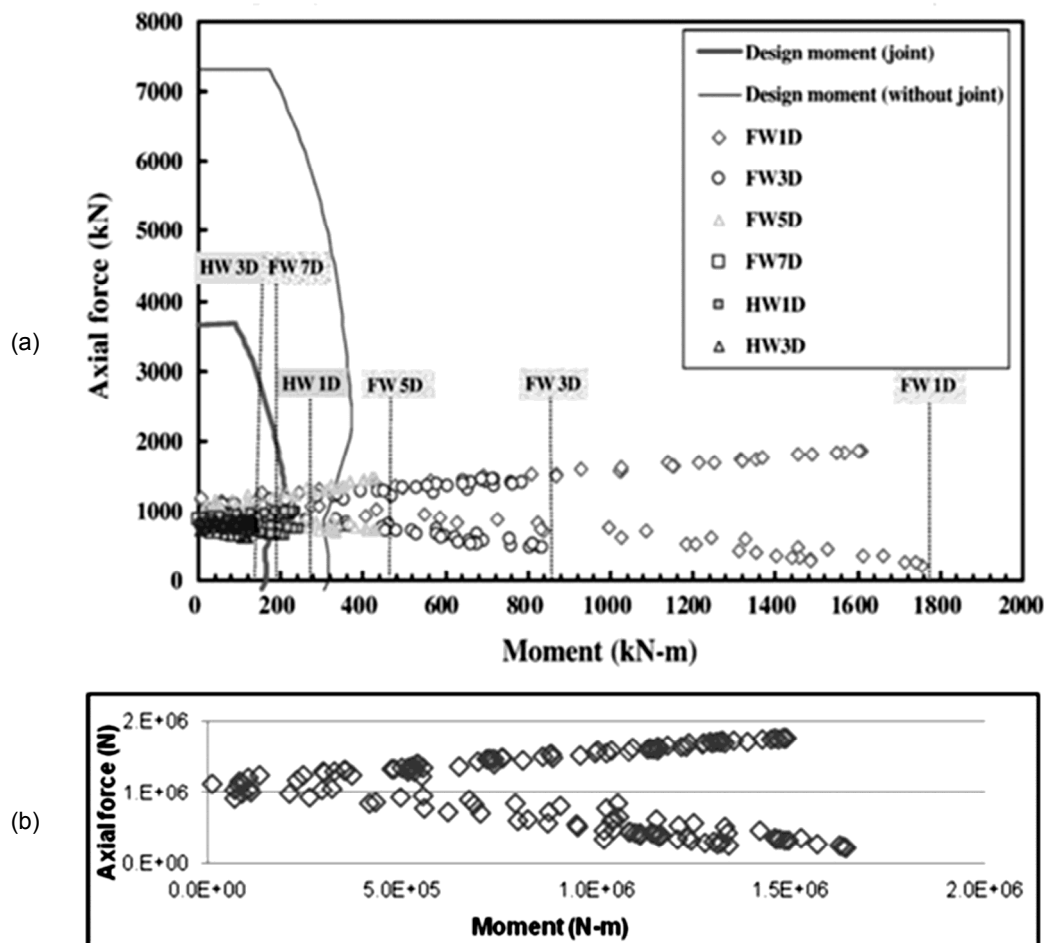


**Fig. 8** The P-M curves of the lining as well as its load state, obtained by (a) Lin et al. (2007), (b) the established numerical model.

(2005). In the developed numerical model, a thrust fault propagated at the dip angle of  $60^\circ$  with a vertical displacement of  $\Delta H/H=0.08$  ( $\Delta H$  is the vertical displacement, and  $H$  is the depth of soil) and a circular tunnel located at  $FWID$  ( $FW$  denotes footwall,  $D$  is the tunnel diameter and  $1D$  denotes the horizontal distance between the lining center and the fault tip line in bedrock). The model configuration is the same as described in Figure 3. The material properties are given in Table 1. As shown in Table 1, the dilation angle of  $30^\circ$  was adopted for verification process. Also, the Table 2 presents the model dimensions. In Figure 8, the  $P$ - $M$  curve (axial load capacity versus moment capacity) obtained for the lining in the established numerical model, corresponds to the one obtained by Lin et al. (2007). As shown in this figure, the axial force and the bending moment of the lining section ranges between 100 to 2000 kN, and zero to 1800 kN.m, respectively. Also, Figure 9 compares the zones of plastic shear strain concentration. The locations of plastic shear strain concentration and the measure of strains in the established numerical model are in a complete agreement with the one obtained by Lin et al. (2007). According to the plastic shear zone, the rupture path bifurcation occurred, as it met the

tunnel, and continued to the surface. The tunnel was confined with the propagated shear zone. This caused an external loading on the tunnel lining and made to displace it.

### 3. NUMERICAL ANALYSIS AND DISCUSSION

This study focused on the effects of both permanent fault displacements and dynamic ground motions on tunnel lining's response, including internal load distribution, displacement, and shear distortion of the lining section under reverse fault rupture at dip angle of  $45^\circ$  and in an earthquake magnitude of 7 (i.e., the imposed fault displacements correspond to earthquake with  $M_s$  7) (see Table 3). It is noteworthy to say that, focusing on the effect of reverse fault rupture with earthquake magnitude of 7, exclusively for a tunnel lining at footwall side with horizontal distance of  $1D$  relative to the fault tip line, attributes to the results of previous related studies by Gharizade Varnusfaderani et al. (2015). In this paper, both two fault types (i.e., normal and reverse fault) with different earthquake magnitudes were studied for different tunnel locations. The important conclusion utilized in the current paper is that the reverse fault with high earthquake magnitude ( $M_s$  7) makes

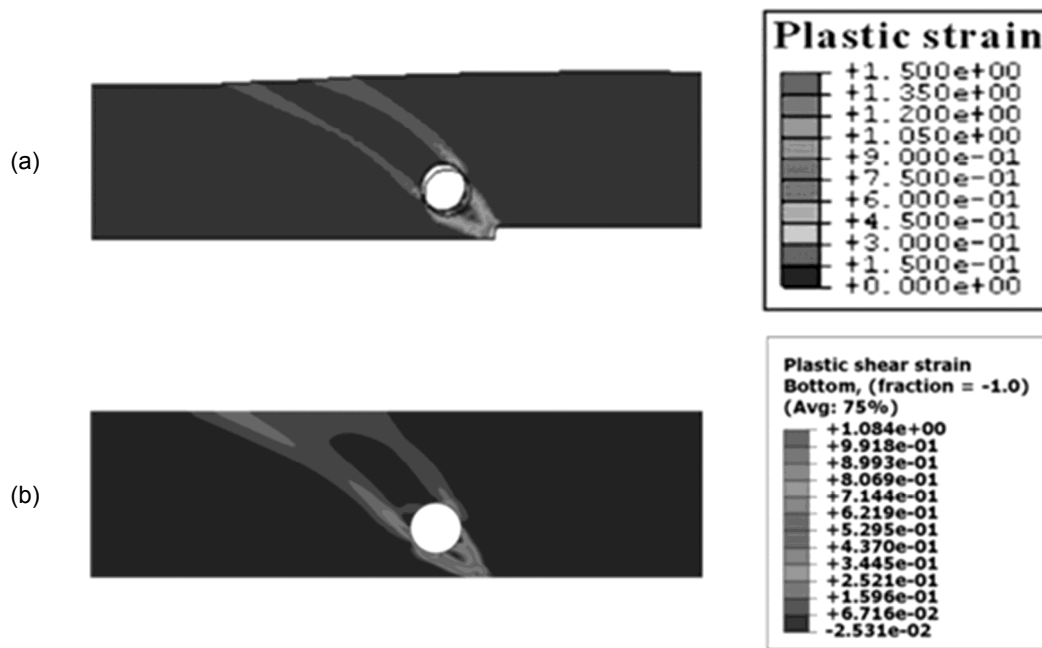


**Fig. 9** The development of shear strain zone, obtained by (a) Lin et al. (2007) and (b) the established numerical model.

a critical structural condition for the lining with the position of *FWID*. Here, the effect of reverse fault on the tunnel lining at *FWID* with different fault dip angles is presented in order to find out critical dip angle. The numerical modeling and analysis procedure corresponds to the last two steps mentioned in Section 2-1. Hence, the numerical results are discussed in two sections. The first section presents only the results of static analysis under the permanent fault dislocation performed on *FWID* case under reverse fault slip at dip angles of  $45^\circ$ ,  $60^\circ$ ,  $75^\circ$ , using the details explained in Section 2-1, step 4 and Section 2-4. The second section presents the results of both the dynamic and quasi-static analysis under the combined primary seismic shaking (using the details explained in Section 2-1, step 3 and Section 2-3) and reverse fault slip at dip angle of  $45^\circ$ . The tunnel was located at a critical position relative to fault rupture, *FWID* case.

### 3.1. TUNNEL BEHAVIOR UNDER APPLIED PERMANENT FAULT DISLOCATION

#### 3.1.1. PLASTIC SHEAR STRAIN

Reverse fault movement and its rupture in soil are mechanically analogous to a gravity wall under passive condition, with the exception that at steeper fault dip angle (larger than  $45^\circ$ ), its mechanism is similar to vertical uplifting in hanging wall side (Anastasopoulos et al., 2008b). Forming a passive wedge in hanging wall side the fault zone reached the plastic state as shown in Figure 10. In other word, due to existence of the tunnel in shear path (the shear path is prescribed by the closed form solutions), a bifurcation occurred, which is as change in fault rupture mechanism in soil. This event is based on the

principal of minimum work. In fact, the lining stiffness is higher than the soil stiffness. That is why the plastic shear strain path is deviated to the invert and near to the vault of tunnel lining. By increasing the fault dip angle (from  $45^\circ$  to  $75^\circ$ ), the plastic shear zone got relocated farther than the footwall or closer to the hanging wall and the width of the shear zone (i.e., the width of passive wedge) decreased. This is in line with theoretical results, performed by Anastasopoulos et al. (2008b).

#### 3.1.2. SECTIONAL FORCES OF THE TUNNEL LINING

For all fault dip angles, the shear zone passed through *FWID* case or from its side, thus, the plastic shear zone developed around the tunnel, which is why, the asymmetric loading on lining occurred and increased bending moment distribution, changing its direction. Moreover, the bending moment distribution was rotated about 90 degrees, independent of fault dip angle. The maximum bending moment position at  $90^\circ$  of the lining section was transferred to the range of  $0^\circ$  to  $350^\circ$ , passed by shear zone (the apex of the tunnel is on the right side of lining). In each fault dip angle, such a change in axial load was non-uniform. Also, for this case, by increasing fault dip angle and relocating the shear zone farther from the tunnel in footwall, the maximum bending moment decreased (Fig.11).

#### 3.1.3. TUNNEL LINING DISPLACEMENTS

By increasing the fault dip angle in different earthquake magnitudes (referring to per the amount of fault dislocation), both components of the displacement at the tunnel vault and the invert

decreased, while the displacements at the tunnel vault were approximately double in size of the one at the invert; therefore, shear distortion (Table 6) and rotation occurred for tunnel cross-section. Increasing the earthquake magnitudes caused the values of tunnel vault and invert displacements to get closer to each other for larger fault dip angles (Fig. 12).

### 3.2. TUNNEL BEHAVIOR UNDER COMBINATION OF THE APPLIED NEAR FAULT GROUND MOTIONS AND PERMANENT FAULT DISLOCATION

In this section, the time histories of the sectional forces of lining at 45° of the lining section (the zero section corresponds to the apex of the trigonometric circle, located at the right side of the tunnel lining) and the lining distortion (relative horizontal displacement between the tunnel vault and invert) are obtained for different earthquake specifications. Also, these are studied under the subsequent reverse fault rupture at the fault dip angle of 45°. Hereafter, the state of applying seismic excitation combined with

**Table 6** Shear distortion of tunnel cross-section under reverse faulting – cm.

FWID		Fault dip angle - Degree		
		45°	60°	75°
$M_w$ (Richter)	6	-9.41	-9.17	-6.53
	6.5	-9.84	-9.69	-7.27
	7	-10.3	-10.1	-7.87

Remark:

$M_w$ : Earthquake magnitude

Fault dip angle is relative to the horizontal direction-degree.

Shear distortion of the tunnel cross section is based on relative horizontal displacement between tunnel vault and invert- cm.

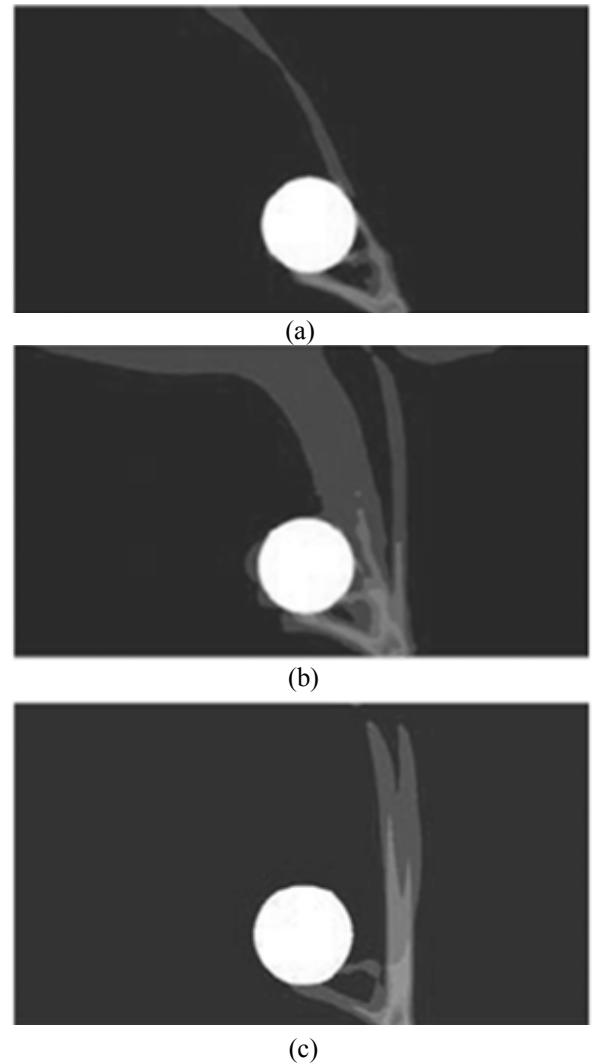


**Fig. 10** Plastic shear strain due to reverse fault rupture in earthquakes with a magnitude of 7 at FWID with dip angles of (a) 45°, (b) 60°, and (c) 75°.

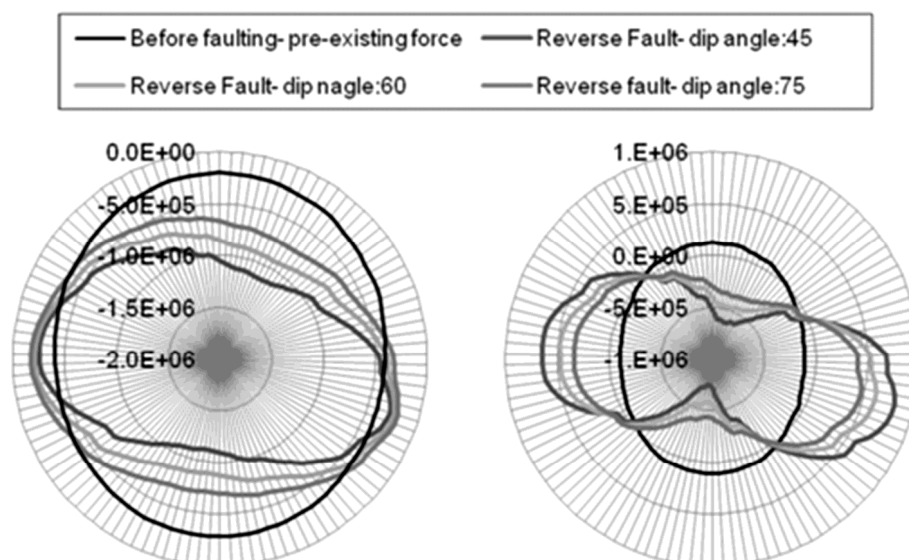


**Fig. 11** The distribution of sectional forces of the tunnel lining under reverse fault slip with dip angles of 45°, 60°, and 75° for FWID cases in an earthquake magnitude of 7 (a) Axial force (N), (b) Bending moment (N.m).

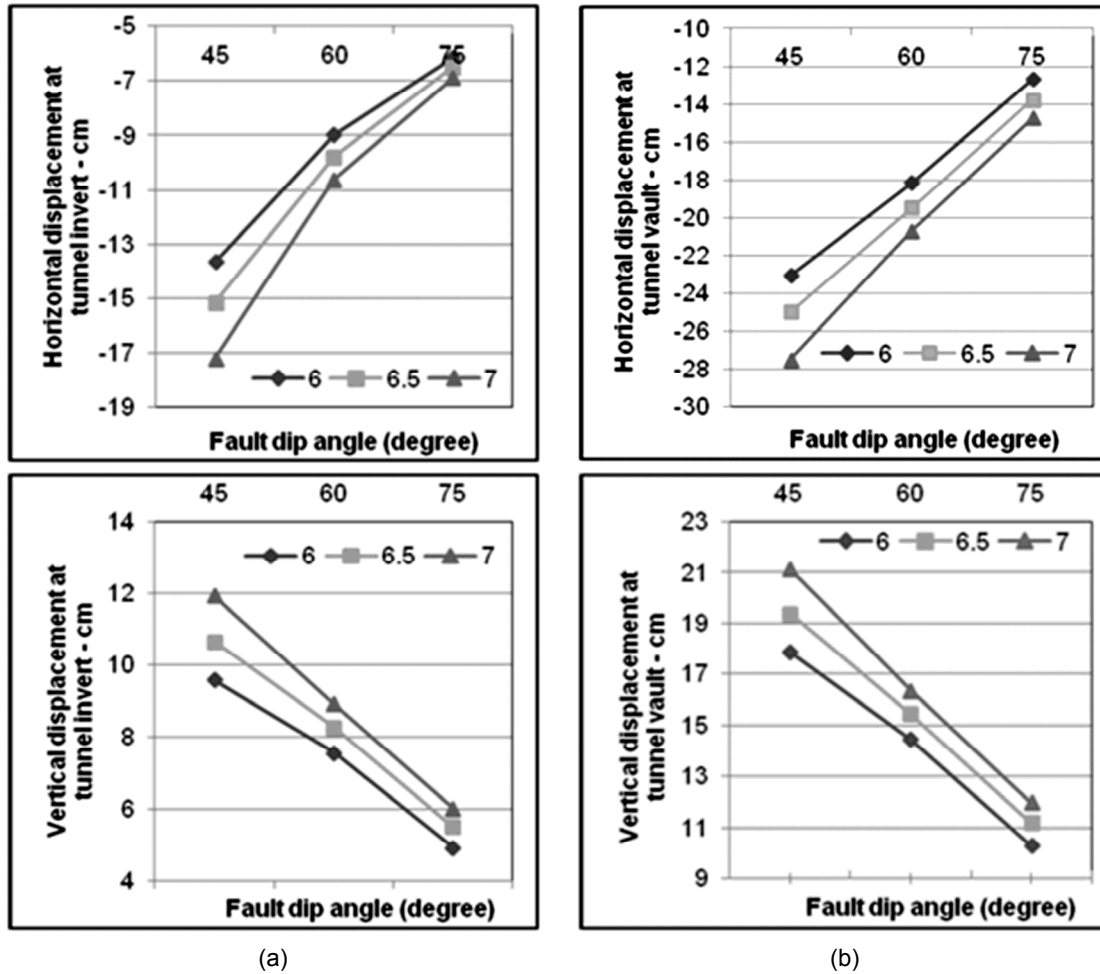


**Fig. 12** The displacements of the tunnel vault and invert versus fault dip angle in different earthquake magnitudes; (a) the displacements at the tunnel invert, (b) the displacements at the tunnel vault (for all diagrams, the negative values of horizontal displacement and positive values of vertical displacements in vertical axis show that the tunnel moved to left side and upward, respectively, this is in accordance with the direction of reverse fault slip).

subsequent fault rupture is called first condition and the state of fault rupture with no primary seismic excitation, second condition. This section aims at studying and comparing the final results obtained by the first and second conditions.

### 3.2.1. THE LINING DISPLACEMENTS

The earthquake time histories are each equivalent to a specified pulse type. Based on the data given in Table 5, the pulse type in Loma-Prieta earthquake is almost like the Type-C one with the two other earthquake time histories similar to the Type-B one. Also, the Loma-Prieta earthquake has the lowest pulse period in comparison to the other two. Assessing the lining behavior, the value of pulse period ( $T_p$ ) was also compared to the fundamental period of the system ( $T$ ). Based on a frequency analysis, the fundamental period of the system is 1.33 seconds. Therefore, the ratio of  $T$  to  $T_p$  for the Northridge, Loma-Prieta, and Cape - Mendocino earthquakes are 0.31, 0.69, and 1.76, respectively. This lining response is expected to be amplified as the

pulse period approaches the fundamental period of the system model (i.e.,  $T_p/T = 1$ ). According to Figure 13 during the seismic loading with  $PGA = 0.35$  g, the lining distortion (i.e. the relative horizontal displacement between tunnel vault and invert) equals to 5 cm, under the primary Loma-Prieta earthquake with  $T_p/T = 0.31$  and  $SV_{max}/PGV = 3.74$ , which is equivalent to Type-C pulse and the lower values by the Northridge and Cape - Mendocino earthquakes (equaling to 3.5 in the former and 3 cm in the latter) with  $T_p/T = 0.69$  and 1.74 and  $SV_{max}/PGV = 2.23$  and 2.41, respectively. The two latter earthquakes are equivalent to Type-B pulse. By increasing the PGA as high as 0.7g and 1g, the maximum lining distortion during the Northridge and Loma-Prieta earthquakes become close values (equaling to 8 and 7.6 cm at  $PGA = 0.7$  g and 9.4 and 9.9 cm at  $PGA = 1$  g respectively). In spite of the fact that the ratio  $T_p/T$  for Northridge earthquake is closer to the unit, the lining distortion is higher in Loma-Prieta earthquake with  $PA = 0.35$  g, independent of the ratio  $T_p/T$ . By increasing the pulse intensity and PGA as high as

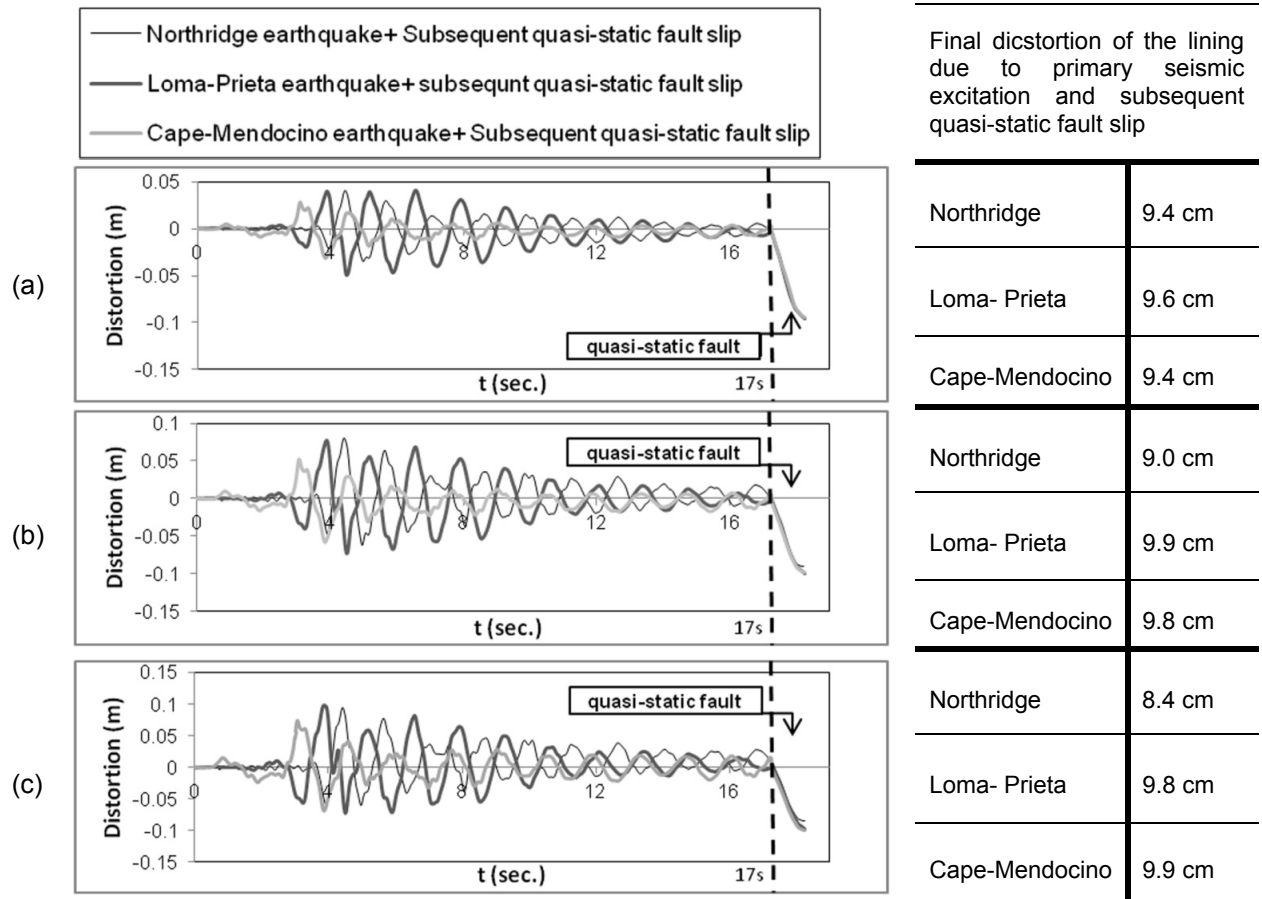


**Fig. 13** The time history of shear distorsion of tunnel lining section under earthquake with PGA (a) 0.35 g, (b) 0.7g, (c) 1 g; the final shear distortion of the tunnel lining equals to 10.31 cm.

0.7 g and 1 g, the ratio  $T_p/T$  plays an important role in lining distortion. These can be attributed to the forward and backward momenta acquired during the forward directivity pulse C- type rather than the pulse B- type, which is effective just at low PGA= 0.35 g, while at PGAs= 0.7 g and 1g, the ratio  $T_p/T$  close to the unit in Northridge earthquake is more effective than the type- C pulse in Loma-Prieta earthquake. Among all, the Cape - Mendocino earthquake makes the lowest lining distortion during the seismic loading, which is equivalent to type B- pulse with the highest ratio  $T_p/T$ . Despite different ranges for the ratio  $T_p/T$ , the final distortion of the lining (i.e., the distortion induced by the first condition) is uniform at each category of earthquakes with PGA= 0.35 g, 0.7 g, and 1 g (Fig. 13).

Due to an elastic behavior assumed for the tunnel lining material, no permanent deformations will be after the near fault earthquakes. Thus, further deformations are induced by the soil - lining interaction (in other words, the soil deformations impress the lining). The displacements induced by the first condition with PGAs = 0.35, 0.7 g, and 1 g, decrease less than 10 percent, in comparison to those induced by the second condition; the final lining distortion due to the second condition is about 10.31 cm. In addition, as a result of increasing stresses at the tunnel vault and the invert due to redistribution

of soil stress and loss of the effect of tunnel construction sequence followed by applying earthquake, the soil shear strength and frictional interaction between the soil and the tunnel lining increase. Consequently, the relative slip between the soil and concrete lining of the tunnel and shearing decrease insignificantly. Generally, by increasing the PGA as high as 0.7 g and 1g, there is no further change in frictional interaction; instead the area of the plastic strain in soil around the tunnel increases. In conclusion, the final permanent displacement of the tunnel induced by the first condition, increases rather than that arising from the second condition, which is due to high PGAs as large as 0.35 g, 0.7 g, and 1 g (Fig. 13).

### 3.2.2. CHANGES IN THE SECTIONAL FORCES OF THE LINING

The internal forces in several sections of the lining have been examined, where only the section at 45 degree of the lining is indicated. Applying strong ground motions (i.e. near fault ground motions) made a monotonic increase in axial load and a periodic change in shear forces of tunnel lining (as diagramed in the first 17 minutes of Figure14a1-2 and Figure14b1-2). In contrast with the two previous sectional forces, the changes in bending moment at different sections are not the same (i.e., depending on

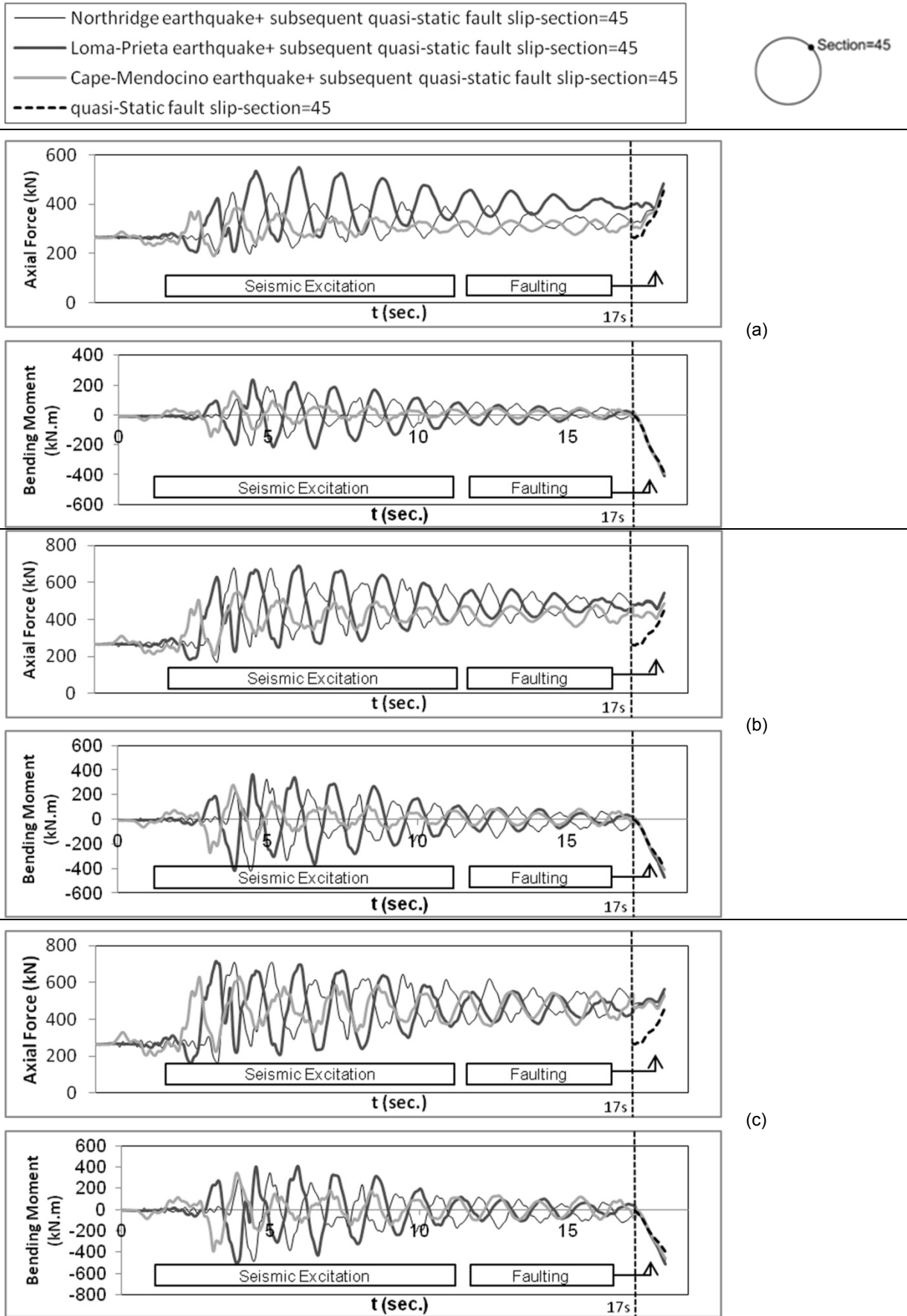


**Fig. 14** The time history of axial load and bending moment of the tunnel lining in different earthquakes with PGA (a) 0.35 g, (b) 0.7 g, (c) 1 g.

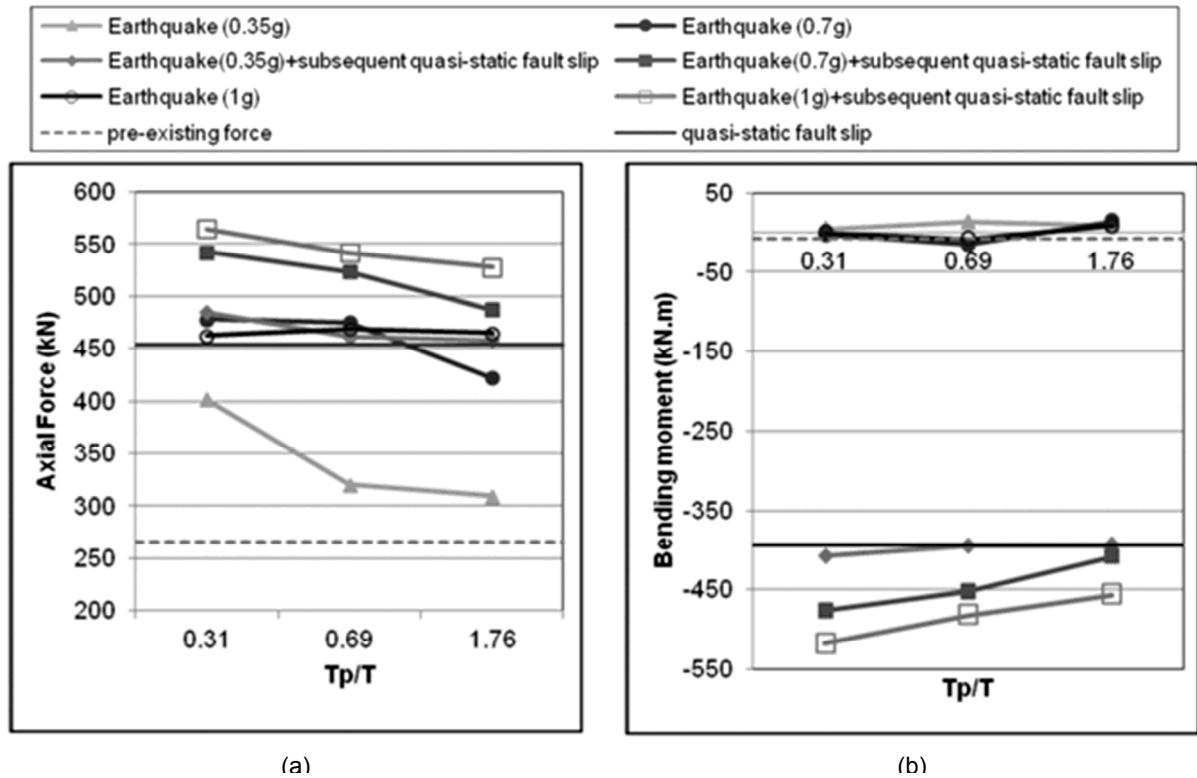


**Fig. 15** The changes of the axial force and bending moment in lining section versus the TP/T ratio at the end of seismic loading and the combination of earthquake and subsequent quasi-static fault slip with different earthquake intensity (PGA) for (a) Axial force, (b) Bending moment.

the angle of the section, it has periodic or monotonic changes) (Figs. 14a, b-3). As aforementioned, there is no sensible permanent deformation after near fault earthquakes with PGA= 0.35 g. While, the amount of plastic strain and the affected zone increases by increasing PGA (the parameter indicating the amplitude of strong ground motions) and high value of PGV, CAV, and IA (the parameters indicating the energy of strong ground motions). Therewith, the sectional forces of the lining increases.

Here, periodic and monotonic variations in bending moment occurred during the seismic loading, but upon completion of the seismic loading, not having permanent asymmetric deformation led not to have considerable ultimate change in bending moment, except for some sections. For earthquakes with PGAs (i.e., 0.35, 0.7 and 1 g) combined with fault rupture, the maximum increase was at 45 ° of the tunnel lining section, which is the same as the results obtained under just fault rupture.

After earthquakes with PGA=0.35 g, the axial load increased between 16 to 50 %, with different earthquakes specifications and the bending moment changed up to 50 %. For earthquakes with PGA = 0.7 g, the axial load and bending moment, both increased between 60 to 80 %. Among the three earthquakes, the Loma-Prieta and Northridge earthquakes have the most effect on the tunnel response, with the lowest one belonging to the Cape-Mendocino earthquake. Although the mentioned increases occurred after the earthquakes, the final axial load and bending moment induced by

combination of the earthquakes with PGA= 0.35 g and subsequent fault rupture was between 1 to 10 % and up to 5 %, respectively, comparing those induced by just fault rupture. In contrast with these, after earthquakes with PGA as high as 0.7g and 1g and subsequent fault rupture, the axial load and bending moment increased between 10 to 30 % and 5 to 20 %, respectively (Figure14).

Evidently, the earthquakes with high spectral velocity response ( $SV_{max}$ ) and high root mean square acceleration ( $a_{rms}$ ) (the parameters both indicates the frequency contents of ground motions) and PGV (the parameter indicates the pulse intensity and applied energy) have larger effects on tunnel response (i.e., the axial and shear forces and bending moment), whether during the seismic excitation or after the subsequent quasi-static displacement of faulting followed by the earthquakes. Such actions are in accord with Loma-Prieta and Northridge earthquakes which have high  $SV_{max}$  (231.21 and 126.82 cm/s, respectively) and lower pulse periods (0.41 and 0.92 s, respectively). That is why these earthquakes made more sensible changes in sectional forces of the tunnel lining (Figure14).

Comparing the influence of pulse type and the ratio  $T_p/T$  on internal forces, final results of the axial force and bending moment in an internal section of the lining at 45°, both at the end of the seismic loading and the combination of the seismic loading with subsequent fault rupture is displayed in Figure 15. As shown in Figure 15a, at PGA = 0.35g, the final axial force, obtained from the Loma-Prieta earthquake

where  $T_p/T = 0.31$  and equivalent Type-C pulse, leads to a high value, unlike that if the Northridge and Cape - Mendocino earthquakes with equivalent Type-B pulse and the ratio  $T_p/T = 0.69$  and  $1.76$ , respectively. At  $PGA = 0.7g$  and  $1g$ , the obtained results by the Northridge and Loma-Prieta earthquakes have close values. By applying fault rupture after the earthquakes with  $PGA = 0.35g$ , these specifications continue, except that for the Northridge and Cape-Mendocino earthquakes, the final results are uniform and unconditioned to the ratio  $T_p/T$  and they have not changed in respect to the obtained results of faulting with no primary seismic excitation. The earthquakes with  $PGA = 0.7g$  and  $1g$  influence the obtained results of subsequent faulting, in which both  $T_p/T$  ratio along with the pulse type are effective factors. According to Figure 15b, uniform changes are made in bending moment after seismic loading with  $PGAs = 0.35$  and  $0.7g$ , unconditional to the pulse type and  $T_p/T$  ratio. By applying subsequent fault rupture, the bending moment is the same as mentioned for the axial force.

#### 4. CONCLUSION

Evaluating the tunnel behavior through internal forces and displacement under a combination of static displacement of faulting and near fault seismic motion was the scope of this study. In order to reach these goals, a finite element program based on 2-D model was adopted. The fault slip (fling step) and near fault excitation (directivity) were applied to the model.

Reverse fault type with an earthquake magnitude of 7, *FWID* tunnel location and near fault ground motions with equivalent pulse characterized by rupture directivity were adopted for the analysis. Considering different aspects of the tunnel position relative to active faults and other types of fault (strike slipping) needs more accurate studies based on 3-D models.

According to the soil properties and the specific tunnel lining structure considered in this study, the results obtained are as follows:

1. The maximum changes in axial load under combined earthquake with  $PGA=0.35$  g and reverse fault rupture, are less than 10 percent. Moreover, the maximum increase for  $PGA=0.7$  g is less than 31 percent.

The maximum increase and decrease in bending moment under combined earthquake with  $PGA = 0.35$  g and fault rupture is less than 5 and 10 percent, respectively, and for the earthquake with  $PGA=0.7$  g is about 10 to 15 and 10 percent, respectively.

The maximum increase and decrease in shear load under combined earthquake with  $PGA=0.35$  g and fault rupture is less than 5 and 10 to 20 percent, respectively. And also for the earthquake with  $PGA=0.7$  g is about 10 to 15 and 10 to 20 percent, respectively.

The final relative displacement of the tunnel lining under combined earthquake with  $PGA=0.35$  g

and fault rupture decreases less than 5 percent, compared to the time that fault rupture occurred with no primary seismic excitation. This is due to the increase in friction between soil and lining, resulting from increasing soil stress.

The final relative displacement of the tunnel lining under combined earthquake with  $PGA = 0.7$  g and fault rupture increased less than 10 percent, compared to the time that the fault rupture occurred with no primary seismic excitation. This is due to an increase in plastic strain around the tunnel resulting from high  $PGA$ .

The pulse type characterized by  $SV_{max}$  and  $PGV$  (indicating the pulse intensity), and the pulse period ( $T_p$ ) play an important role in final response of the tunnel lining (i.e., sectional forces and displacement). In earthquake with low  $PGA$  and small values in near source seismic parameters, the pulse type governs the final results. So, pulse type-C due to larger number of forward and backward momentum rather than pulse type-B, is influential on final results, obtained by subsequent fault slip; Instead, for earthquakes with high  $PGA$  and larger values in near source seismic parameters, the  $T_p/T$  ratio along with the pulse type are important factors affecting the final response of the tunnel lining.

The obtained results shows that the axial force are dependent on the pulse type and  $T_p/T$  ratio, whether during seismic loading or after fault rupture, while the bending moments are opposite during the seismic loading and increase just by increase of the earthquake intensity. The final results of bending moment induced by the combination of near fault earthquake and fault rupture is the same as the axial force.

Considering elastic behavior for lining material did not assess the lining behavior after the earthquake and subsequent quasi- static fault slip comprehensively. Nevertheless, assuming elastic behavior for concrete material, the lining response impressed by the pulse type and  $T_p/T$  ratio, same as the sectional forces. Losing the lining deformations induced by the seismic loading did not lead to extreme changes in final distortion induced by the subsequent fault slip.

For future researches, it is recommended to study the tunnel behavior by considering plastic behavior for concrete materials to investigate final response and distortions of the tunnel structure noting the soil-tunnel interaction.

#### REFERENCES

- Alavi, B. and Krawinkler, H.: 2000, Consideration of near-fault ground motion effects in seismic design. The 12<sup>th</sup> World Conference on Earthquake Engineering.
- Anastasopoulos, I., Gerolymos, N., Drosos, V., Geogarakos, T., Kourkoulis, R. and Gazetas, G.: 2008a, Behavior of deep immersed tunnel under combined normal fault rupture deformation and subsequent seismic shaking. *Bull. Earthquake Eng.*, 6, No. 2, 213–239. DOI 10.1007/s10518-007-9055-0

- Anastasopoulos, I., Gerolymos, N., Gazetas, G. and Bransby, M.F.: 2008b, Simplified approach for design of raft foundations against fault rupture. Part I: free-field. *Earthquake Engineering and Engineering Vibration*, 7, 147–163.  
DOI: 10.1007/s11803-008-0835-6
- Anastasopoulos, I. and Gazetas, G.: 2010, Analysis of cut-and-cover tunnels against large tectonic deformation. *Bull. Earthquake Eng.*, 8, No. 2, 283–307.  
DOI 10.1007/s10518-009-9135-4
- Bommer, J.J. and Mendis, R.: 2005, Scaling of spectral displacement ordinates with damping ratios. *Earthquake Engineering and Structural Dynamics*, 34, 2, 145–165. DOI: 10.1002/eqe.414
- Bray, J.D. and Rodriguez-Marek, A.: 2004, Characterization of forward directivity ground motions in the near fault region. *Soil Dynamic and Earthquake Engineering*, 24, 815–828. DOI: 10.1016/j.soildyn.2004.05.001
- Chung, C.F., Lin, M.L., Jeng, F.S., Tsai, L.S., Chin, C.T. and Chan, S.J.: 2005, A case study on the response of shield tunnel near a thrust fault offset. *Proceedings of Geotechnical Earthquake Engineering. Satellite Conference*, Osaka, Japan.
- Corigliano, M., Scandella, L., Lai, C.G. and Paolucci, R.: 2011, Seismic analysis of deep tunnels in near fault conditions: a case study in Southern Italy. *Bull. Earthquake Eng.*, 9, 975–995.  
DOI 10.1007/s10518-011-9249-3
- Cox, K.E. and Ashford, S.A.: 2002, Characterization of large velocity pulses for laboratory testing. Report PEER 2002.22.
- Dowding, C.H. and Rozen, A.: 1978, Damage to rock tunnels from earthquake shaking. *ASCE, Journal of the Geotechnical Engineering*, 104, No. GT2, 175–191.
- Einstein, H.H. and Schwartz, C.W.: 1979, Simplified analysis for tunnel supports. *Journal of the Geotechnical Engineering Division*, 105, ASCE GT4, 499–518.
- Golser, H. and Schubert, W.: 2003, Application of numerical simulation at the tunnel site. In G. Beer (Ed.), *Numerical Simulation in Tunnelling*, 427–474, Wien, Springer-Verlag.
- Jaky, J.: 1944, The coefficient of Earth pressure at rest. *Journal for Society of Hungarian Architects and Engineers*, 355–358.
- Jennings, P.C.: 1985, Ground motion parameters that influence structural damage. In: Scholl, R.E. and King, J.Ll, editors. *Strong Ground Motion Simulation and Engineering Applications*, EERI Publication 85-02. Earthquake Engineering Research Institute, Berkeley, California, USA.
- Krawinkler, H. and Alavi, B.: 1998, Development of improved design procedures for near-fault ground motions. SMIP98, Seminar on Utilization of Strong Motion Data. Oakland, CA, USA.
- Lin, M.L., Chung, C.F., Jeng, F.S. and Yao, T.C.: 2007, The deformation of overburden soil induced by thrust faulting and its impact on underground tunnels. *Engineering Geology*, 92, 110–132.  
DOI: 10.1016/j.enggeo.2007.03.008
- Makris, N.: 1997, Rigidity- plasticity-viscosity: Can electro rheological dampers protect base-isolated structures from near-source ground motions. *Earthquake Engineering and Structural Dynamics*, 26, 571–591.  
DOI: 10.1002/(SICI)1096-9845(199705)26:5<571: AID-EQE658>3.0.CO;2-6
- Maniatakis, Ch.A., Taflampas, I.M. and Spyarakos, C.C.: 2008, Identification of near-fault earthquake record characteristics. The 14<sup>th</sup> World Conference on Earthquake Engineering.
- Martinez-Pereira, A. and Bommer, J.J.: 1998, What is the near-field. 6th SECED Conference on Seismic Design Practice into the Next Century, 245–252.
- Mavroeidis, G. and Papageorgiou, A.: 2003, A mathematical representation of near-fault ground motions. *Bulletin of the Seismological Society of America*, 93, 3, 1099–1131. DOI: 10.1785/0120020100
- Muir Wood, A.M.: 1975, The circular tunnel in elastic ground. *Geotechnique*, 25, 115–127.  
DOI: 10.1680/geot.1975.25.1.115
- Pacific Earthquake Engineering Research Center (PEER). PEER Strong Motion Database. Internet Website: <http://peer.berkeley.edu>
- Panet, M.: 1978, Stability analysis of a tunnel driven in a rock mass in tracking account of the post-failure behavior. *Rock Mechanics*, 8, 1, 209–223.
- Power, M.S., Rosidi, D. and Kaneshiro, J.Y.: 1998, Seismic vulnerability of tunnels and underground structures revisited 1998. *Proceeding of North American Tunneling '98*. Newport Beach, CA: Balkema, Rotterdam, 243–250.
- Schwartz, C.W. and Einstein, H.H.: 1980, Improved design of tunnel supports: Volume 1 - Simplified analysis for ground-structure interaction in tunneling. Cambridge, MA: Massachusetts Institute of Technology, 450 pp.
- Somerville, P. and Graves, R.: 1993, Conditions that give rise to unusually large long period ground motions. *The structural design of tall buildings*, 2, 211–232.  
DOI: 10.1002/tal.4320020304
- Somerville, P.G., Smith, N.F., Graves, R.W. and Abrahamson, N.A.: 1997, Modification of empirical strong ground motion attenuation relations to include the amplitude and duration effects of rupture directivity. *Seismological Research Letters*, 68, 1, 199–222. DOI: 10.1785/gssrl.68.1.199
- Somerville, P.: 2002, Characterizing near fault ground motion for the design and evaluation of bridges. *Proceedings of the Third National Conference and Workshop on Bridges and Highways*, Portland, Oregon, April 29 – May 1, 2002.
- Somerville, P.G.: 2003, Magnitude scaling of the near fault rupture directivity pulse. *Physics of the Earth and Planetary Interiors*, 137, 201–212.  
DOI: 10.1016/S0031-9201(03)00015-3
- Stewart, J.P., Chiou, S.J., Bray, J.D., Graves, R.W., Somerville, P.G. and Abrahamson, N.A.: 2001, Ground motion evaluation procedures for performance-based design. Report PEER 2001/09.
- Terzaghi, K.: 1934, *Theoretical Soil Mechanics*. John Wiley & Sons.
- Varnusfaderani, M.G., Golshani, A. and Nemati, R.: 2015, Behavior of circular tunnels crossing active faults. *Acta Geodyn. Geomater.*, 12, No. 4 (180), 363–376.  
DOI: 10.13168/AGG.2015.0039
- Wells, D. and Coppersmith, K.: 1994, New empirical relationships among magnitude, rupture length, rupture width, rupture area and surface displacement. *Bulletin of the Seismological Society of America*, 84, No. 4, 974–1002.

## APPENDIX A

### **NUMERICAL MODELING OF TUNNEL EXCAVATION WITH STRESS RELEASE METHOD**

The excavation of a tunnel is a three dimensional problem. In this study, it is required the excavation to be simulated in plane strain condition. Actually, to get more realistic results, operating with a two dimensional model, the so called "3D effect" can be simulated by two methods (Golser and Schubert, 2003; Schwartz and Einstein, 1980):

1. Load reduction method ( $\beta$ -method)
2. Stiffness reduction method ( $\alpha$ -method)

As it is usual in tunneling, displacement occurring in the ground before the support can be applied. This displacement mobilizes the resistance of the ground and reduces the load, which the later installed support must carry.

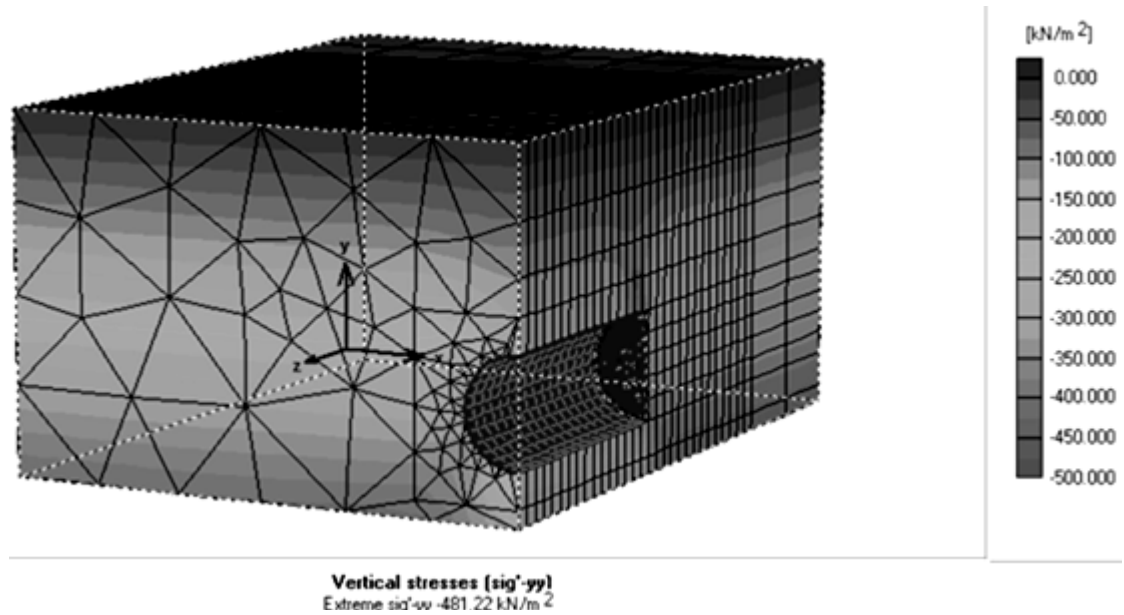
Here, the load reduction method was used to model the tunnel excavation. In the load reduction method (Panet, 1978), an initial state is assumed, where the internal pressure ( $p_0$ ) in this opening equals the external Earth pressure. Before the concrete shell is included, this internal pressure is reduced by a  $\beta$ -factor called stress release ratio or relaxation factor.

The magnitude of the  $\beta$ -factor that corresponds to reality must be obtained from field measurements or numerical studies. In this study, using the last method, a three dimensional excavation model was developed by PLAXIS 3D tunnel software with finite element based method. The tunneling is a TBM based excavation approach. By this way, a twelve phase analysis was performed. Actually, the first ten phases were developed to reduce the model boundary effects and get close to real condition. Each steps of excavation and lining installation was performed in two phase. At the first phase, the tunnel section with 1 m length was removed and the lateral pressure was applied to the excavation face operating by the machine. The mentioned lateral pressure was calculated on the base of Terzaghi's theory (Terzaghi, 1934). And the second phase, the concrete shell was installed. By the tunneling process, the real vertical displacement of the tunnel crown section recorded, for the last phase before lining installation. Then, the 2D numerical model was developed by trial and error in relaxation factor, so that the corresponding displacement was obtained. Finally, the relaxation factor equals to 0.4 (i.e., release of 40 % of unbalanced forces) made a good agreement between 2D and 3D numerical results (Fig. A1 and Fig. A2).

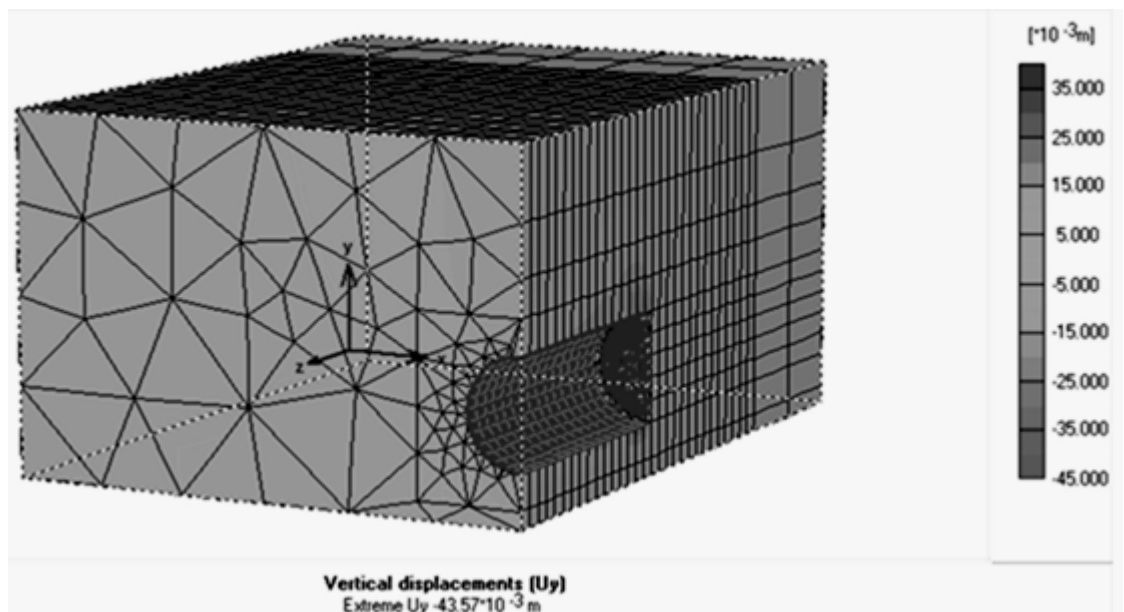
## APPENDIX B

### **DISPLACEMENT TIME HISTORIES OF THE EARTHQUAKES**

The displacement time histories are derived from the corresponding scaled acceleration time histories. Here, the used displacement time histories are presented in Figure B1 to Figure B3, according to different scaled PGAs 0.35 g, 0.7 g and 1 g.



(a)



(b)

**Fig. A1** The results of 3D tunnel excavation model (a) contours of vertical stresses, (b) contours of vertical displacement.

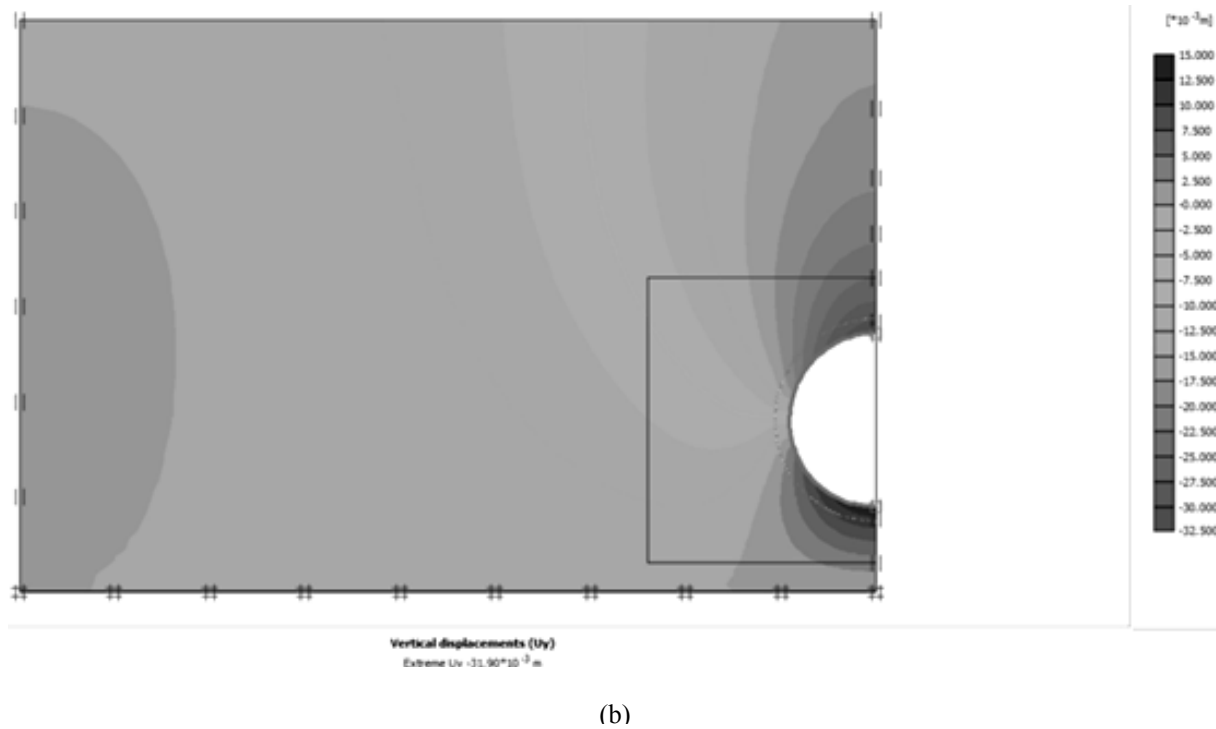
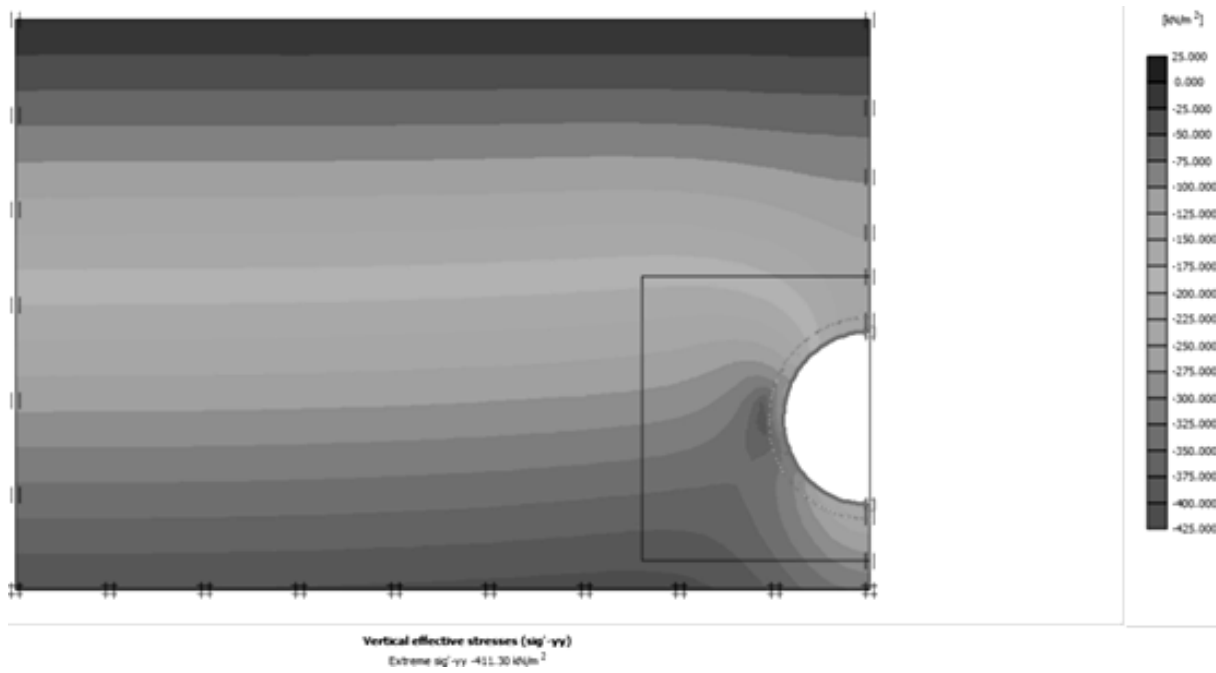


**Fig. A2** The results of 2D tunnel excavation model (a) contours of vertical stresses, (b) contours of vertical displacement.

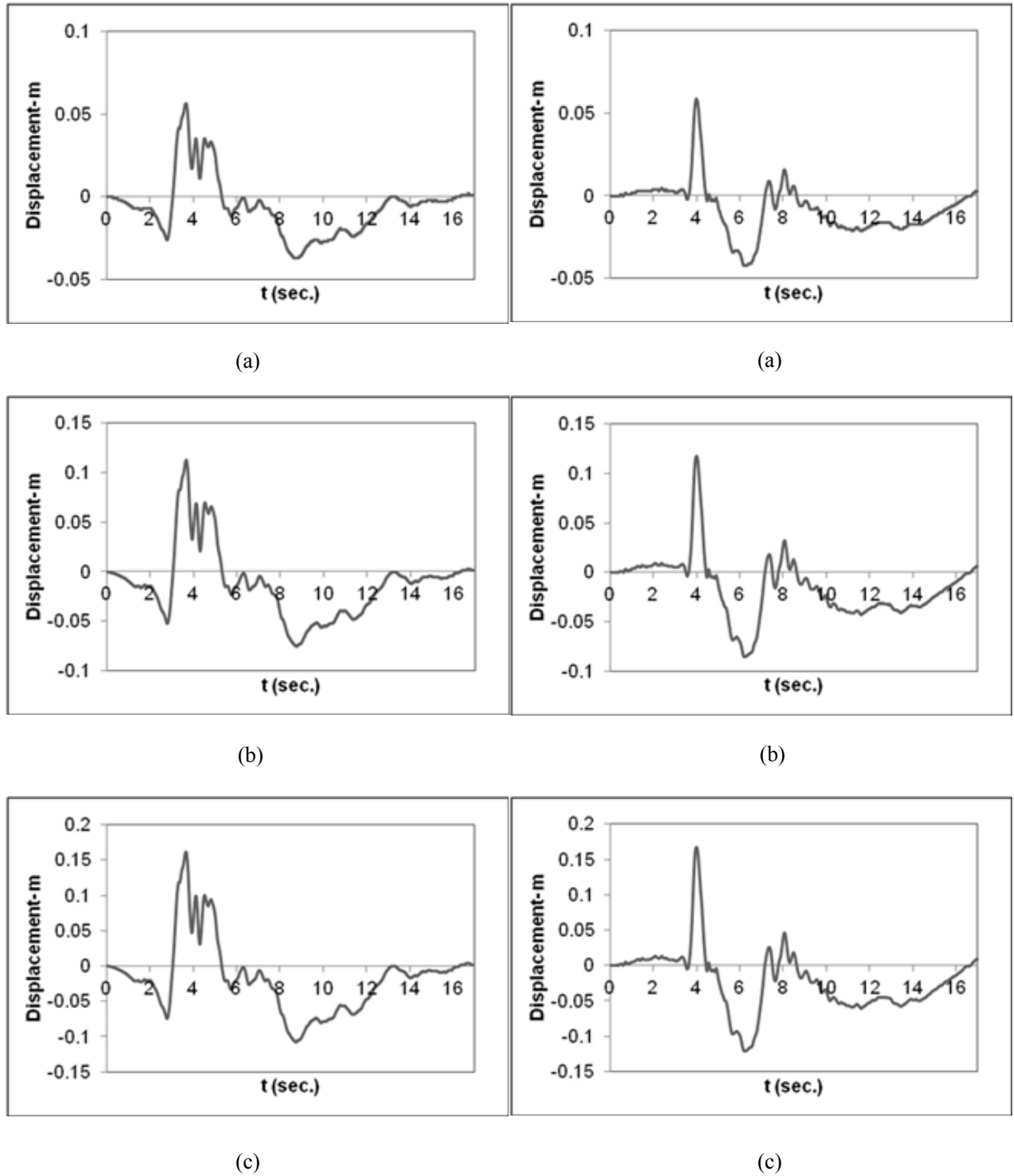


**Fig. B1** The time history of displacement for the Loma-Prieta earthquake with scaled PGAs (a) 0.35 g (b) 0.7 g (c) 1 g.

**Fig. B2** The time history of displacement for the Northridge earthquake with scaled PGAs (a) 0.35 g (b) 0.7 g (c) 1 g.

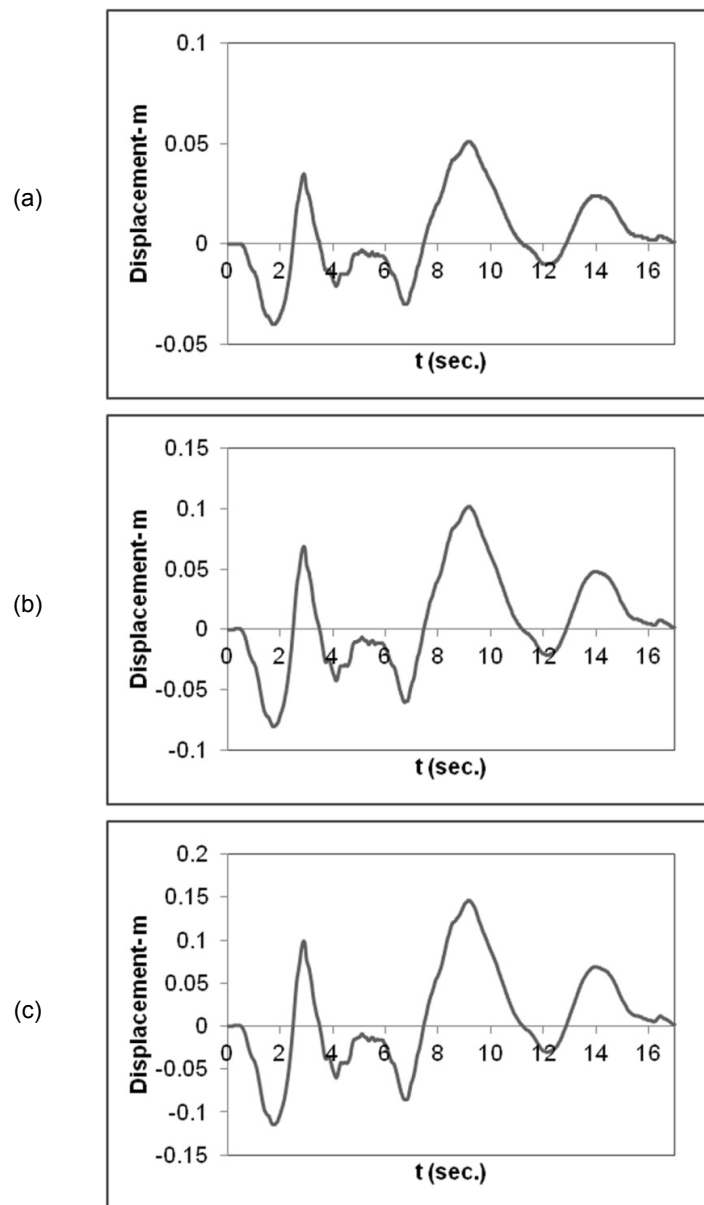


**Fig. B3** The time history of displacement for the Cape-Mendocino earthquake with scaled PGAs (a) 0.35 g (b) 0.7 g (c) 1 g.